Magnetic Resonance in Medicine 42:454–460 (1999)

A Localized Double-Quantum Filter for In Vivo Detection of Taurine

Hao Lei[1] and James Peeling[1,2]*

Noninvasive detection of taurine, an important amino acid involved in numerous physiological processes, by in vivo ^{1}H magnetic resonance (MR) spectroscopy is complicated by severe overlap of the taurine resonances with those of a number of other metabolites. Unambiguous differentiation of the taurine resonances requires spectral editing. In this study, the development of a localized spectral editing technique based on double-quantum filtering optimized for in vivo detection of taurine is described. The sequence recovers the taurine signal while substantially eliminating overlapping resonances and provides excellent three-dimensional spatial localization. The performance of the sequence is demonstrated both in phantoms and in rat brain in vivo. Magn Reson Med 42:454–460, 1999. © **1999 Wiley-Liss, Inc.**

Key words: taurine; double-quantum filtering; magnetic resonance spectroscopy; spectral localization; spectral editing

Taurine is an important metabolic product of sulfur amino acid catabolism (1–3). Taurine has been observed in vivo by using both conventional one-dimensional (1D) and two-dimensional (2D) magnetic resonance (MR) spectroscopy (4–9). Severe overlap of the taurine resonances and the resonances of other metabolites such as choline, *myo*-inositol, and glucose hinders direct observation of taurine with conventional 1D MR spectroscopy (4). 2D J-correlated spectroscopy (COSY) can resolve overlapping resonances from different metabolites, and its use in selective detection of taurine has been demonstrated (7–9). One shortcoming of 2D COSY spectroscopy is that the acquisition time required can be very long, making it unacceptable for many in vivo applications.

A difference double-resonance spectral editing technique has been used to observe taurine in vivo (10). Gradient-selected double-quantum (DQ) filtering, in which MR signals from the target metabolite(s) are selected by using a pair of coherence transfer pathway selection gradient pulses (11), acquires edited signals in a single shot. It is thus less susceptible to motion artifacts and more suitable for in vivo applications than editing methods requiring subtraction of serially obtained spectra. DQ-filtering methods have been applied to the selective observation of lactate (12,13), γ-aminobutyric acid (GABA) (14), citrate (15), glucose (16), *N*-acetylaspartate (17), and glutamate (18) in vivo. A nonlocalized DQ-filtering sequence for taurine editing has been described and demonstrated in rat brain extracts and homogenates (19). A DQ-filtering taurine-editing sequence incorporating spatial localization is described here, and its performance is demonstrated in phantoms and in rat brain in vivo.

MATERIALS AND METHODS

MR experiments were performed on a Bruker Biospec/3 spectrometer with a 7-T, 21-cm magnet equipped with actively shielded gradient coils. A home-built 3-cm-diameter RF saddle coil was used for both transmission and reception. For all experiments, the flip angles of the RF pulses were carefully calibrated (20).

Pulse Sequence

The localized DQ-filtering sequence for taurine editing is shown in Fig. 1. The last five pulses comprise the DQ filter (11). Spatial localization in the slice direction is achieved by making the second 180° refocusing pulse of the DQ filter slice selective (12,14). The two slice-selective hyperbolic secant pulses (21) inserted before the first 90° pulse of the DQ filter provide 2D in-plane spatial localization in a manner that resembles imaging selected in vivo spectroscopy (ISIS) (22).

Phantom Experiments

Four phantoms were used. Each consisted of a 2.5-cm-diameter vial filled with 20 mM taurine in normal saline. For phantoms 2, 3 and 4, a 1.2-cm-diameter vial was inserted concentrically into the larger vial. The inner vial of phantoms 2 and 3 contained choline, GABA and *myo*-inositol, 20 mM each, and 2 mM lactate, in normal saline. The inner vial of phantom 3 also contained 20 mM taurine. The inner vial phantom 4 contained 20 mM glucose in normal saline.

Phantom 1 was used to determine the dependence of the taurine detection sensitivity on the duration of the DQ coherence creation period (2τ) and on the flip angle (θ) of the DQ read pulse. These measurements were made without spatial localization by using 1024 data points, a spectral bandwidth of 4000 Hz, repetition time (TR) = 2.0 sec, and 32 averages. Hard 180° pulses were used as the refocusing pulses, and a 12-msec single-lobe sinc pulse with a bandwidth of 90 Hz was used as the DQ coherence read pulse. Spoiling gradients and coherence transfer pathway selection gradients were adjusted experimentally to a near magic-angle setting to maximize the efficiency of water suppression (23). The DQ evolution time t_1 was kept as short as possible (7.5 msec) to minimize signal loss through so-called J-modulation (11). The detection periods τ_1 and τ_2 were set to $\tau - t_1$ and $\tau + t_1$, respectively, in order to simultaneously refocus the taurine coherence transfer-

[1]Department of Chemistry, University of Manitoba, Winnipeg, Manitoba, Canada.
[2]Department of Radiology, University of Manitoba, Winnipeg, Manitoba, Canada.
Grant sponsors: Research Partnership Program of the Natural Sciences and Engineering Research Council; the National Research Council of Canada; Astra Pharma.
*Correspondence to: James Peeling, Department of Pharmacology and Therapeutics, University of Manitoba, 770 Bannatyne Avenue, Winnipeg, Manitoba, Canada R3E 0W3. E-mail: jpeeling@ms.umanitoba.ca
Received 3 February 1999; revised 8 June 1999; accepted 8 June 1999.

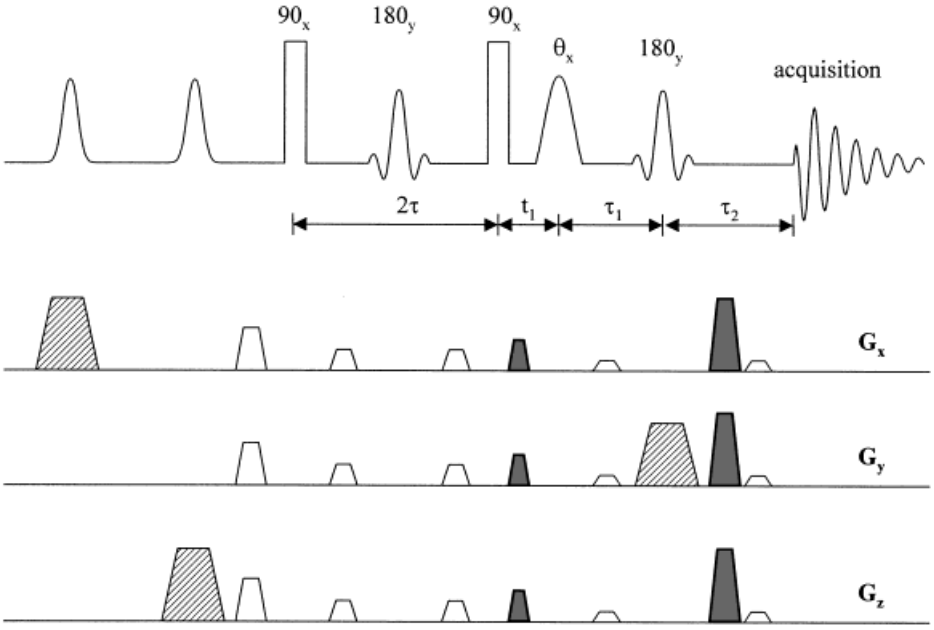

FIG 1. Double-quantum filtering pulse sequence for taurine editing, incorporating three-dimensional spatial localization. The first two hyperbolic secant pulses are for spatial localization, and the remaining five pulses form the double-quantum filter. For taurine editing, 2τ = 37.5 msec, t_1 = 7.5 msec, τ_1 = 11.25 msec, τ_2 = 26.25 msec. The amplitudes of the gradient pulses for spatial localization (hatched box), double-quantum filtering (shaded box), and spoiling (open box) are adjusted to avoid the formation of gradient echoes.

echo and the B_o inhomogeneity experienced by the taurine DQ coherence during the t_1 period (11). With $\theta = 90°$, the intensity of the DQ filtered taurine signals was measured as 2τ was varied in 50 steps from 30 to 210 msec. With the optimum value of 2τ (37.5 msec) determined from these experiments, the DQ filtered taurine peak intensity was measured as θ was taken through 22 steps from 5° to 150°. All subsequent taurine-edited spectra were acquired with the resulting optimized values of 2τ and θ (60°).

For experiments involving spatial localization, scout images were obtained with a snapshot fast low-angle shot (FLASH) imaging sequence (24). Volume-localized nonedited ^{1}H MR spectra were acquired with a stimulated echo acquisition mode (STEAM) sequence (25) with a voxel size of $5 \times 5 \times 5$ mm^3. Each STEAM spectrum was obtained with 128 transients acquired into 2048 data points with a spectral bandwidth of 2500 Hz, TR = 2.0 sec, echo time (TE) = 20 msec, and mixing time (TM) = 30 msec. Volume-localized taurine-edited ^{1}H MR spectra were acquired with the pulse sequence shown in Fig. 1 with a spectral bandwidth of 4000 Hz and TR = 2.0 sec. Thirty-two averages were accumulated into 1024 data points for each of the four ISIS-like steps, resulting a total of 128 acquisitions. Hyperbolic secant pulses (5 msec) with a bandwidth of 2200 Hz were used as the inversion pulses for spatial localization, and 1-msec sinc-gaussian pulses (half-width at half-maximum) were used as the refocusing pulses. The read pulse, gradients, t_1, τ_1, and τ_2 were adjusted as described above.

For both the STEAM and the taurine-edited spectra, postacquisition processing included zero-filling the free induction decays (FIDs) to 4096 data points and applying 5-Hz exponential line broadening before Fourier transformation.

In Vivo Experiments

Three male Sprague-Dawley rats weighting 275–325 g were used. Each rat was anesthetized with 1.0–1.5% halothane in 30/70 O_2/N_2O administered via a nose cone. Rectal temperature was controlled at 36.5–37.5 °C using a thermostated water blanket. For each rat, a volume-localized STEAM spectrum was obtained from an $8 \times 8 \times 5$ mm^3 voxel centered in the brain, with 128 transients acquired into 2048 data points, a spectral bandwidth of 2500 Hz, TR = 2.0 sec, TE = 20 msec, and TM = 30 msec. Localized taurine-edited spectra were acquired from the same voxel by using the parameters described above for the phantom experiments. FIDs were zero-filled to 4096 data points and line-broadened by 15 Hz prior to Fourier transformation.

DQ Signal Intensity Simulations

Product operator formalisms were used to simulate the intensity of the DQ filtered taurine signal as a function of 2τ and θ (26,27). For a DQ-filtering sequence with $\tau_1 + \tau_2 = 2\tau$, the 2τ dependence of the fractional signal intensity passing through the DQ filter for a strongly coupled AB system is (15)

$$f(2\tau) = \frac{1}{2}\left\{\left[\left(\frac{\Delta\omega}{\Lambda}\right)^2 + \left(\frac{\pi J}{\Lambda}\right)^2 \cos(2\Lambda\tau)\right]\sin(2\pi J\tau) - \left(\frac{\pi J}{\Lambda}\right)\sin(2\Lambda\tau)\cos(2\pi J\tau)\right\}^2 \exp\left(\frac{-4\tau}{T_2}\right) \quad [1]$$

where $\Delta\omega = (\omega_A - \omega_B)/2$ is the one-half the chemical shift difference (in rad·sec^{-1}) between A and B and $\Lambda = [\Delta\omega^2 + \Delta\omega^2 + (\pi J)^2]^{1/2}$ is the strong coupling frequency. For a weakly coupled A_2X_2 spin system, $f(2\tau)$ is identical to that for an AX system except that the period of the sin/cos modulation for the A_2X_2 system is twice that for an AX spin system (28). Assuming this applies to strongly coupled spins systems, $f(2\tau)$ for the A_2B_2 system of taurine ($\Delta\omega$ =

160.3 rad · sec^{-1} at 7 T, J = 6.7 Hz) (29) can be written

$$f(2\tau) = \frac{1}{2}\left\{\left[\left(\frac{\Delta\omega}{\Lambda}\right)^2 + \left(\frac{\pi J}{\Lambda}\right)^2 \cos(4\Lambda\tau)\right]\sin(4\pi J\tau) - \left(\frac{\pi J}{\Lambda}\right)\sin(4\Lambda\tau)\cos(4\pi J\tau)\right\}^2 \exp\left(\frac{-4\tau}{T_2}\right) \quad [2]$$

where T_2 is the transverse relaxation time for taurine.

When a ''non-frequency-selective'' read pulse and a DQ coherence selection gradient pair of the same polarity are used, the fractional signal intensity passing through the DQ filter as a function of θ for an AX (27) or an AB (15) system is

$$f(\theta) = \sin(\theta)\cos^2\left(\frac{\theta}{2}\right). \quad [3]$$

Eqs. [2] and [3] were used to simulate the DQ-filtered taurine peak intensity as a function of 2τ and θ.

RESULTS

Figure 2 shows the normalized intensity of the taurine signal passing through the DQ filter as a function of the DQ creation time 2τ (Fig. 2a) and the flip angle θ of the DQ read pulse (Fig. 2b). Over the observable range, the experimental intensity of the taurine signal is maximum at 2τ = 37.5 msec (Fig. 2a), with two additional local maxima at 2τ = 112.5 and 185.0 msec and two local minima at 2τ = 75.0 and 150.0 msec. The product operator simulation reproduces the experimental features for 2τ < 180 msec; in particular, the position of the calculated intensity maximum, lower local maxima, and local minima agree with experiment. The experimental intensity of the taurine signal is maximum when θ = 60° (Fig. 2b), higher by a factor of 1.30 than the intensity for θ = 90°; this is reproduced by the simulation.

Figure 3 shows localized nonedited (Fig. 3a and c) and taurine-edited (Fig. 3b and d) spectra acquired from identical voxels in the inner vials of phantoms 2 (Fig. 3a and b) and 3 (Fig. 3c and d). No taurine resonances at 3.43 and 3.27 ppm are apparent in the spectra in Fig. 3a or b, indicating that effective localization is achieved. With taurine editing, the intense choline methyl singlet (3.20 ppm) is effectively suppressed (Fig. 3b and d), as are the *myo*-inositol peaks between 3.20 and 3.50 ppm (Fig. 3b). However, the GABA triplet at 3.00 ppm, the *myo*-inositol multiplets between 3.50 and 3.70 ppm, and the *myo*-inositol [H2] and choline methylene peaks at 4.06 ppm remain in the spectrum, all with modulated phase. The spectrum in Fig. 3d shows taurine signals at 3.43 and 3.27 ppm in addition to the background signals shown in Fig. 3c.

Nonedited and taurine-edited spectra acquired from the same voxel located in the inner vial of phantom 4 are shown in Fig. 4a and b, respectively. Figure 4c shows a taurine-edited spectrum acquired from a voxel with the same size located in the outer vial of the same phantom. Comparing the integrated intensity between 3.10 ppm and 3.50 ppm in the spectra in Fig. 4b and c, the relative detection sensitivity of the DQ-filtering sequence for glucose and taurine is approximately 1:8.

Figure 5 compares taurine-edited spectra acquired by using the sequence in Fig. 1 (Fig. 5a) with taurine-edited spectra obtained by using a DQ-filtering sequence incorporating Gaussian pulses for excitation and DQ coherence creation and a hard 90° pulse for the read pulse (Fig. 5b) (19). The two spectra were acquired from the same voxel located in the inner vial of phantom 3. Common acquisition parameters were kept the same, and other parameters for each pulse sequence were carefully adjusted to give the maximum taurine signal intensities. The spectrum in Fig. 5b shows less contamination with resonances of GABA, choline, and *myo*-inositol, but at the cost of a reduction in signal intensity of about 42%.

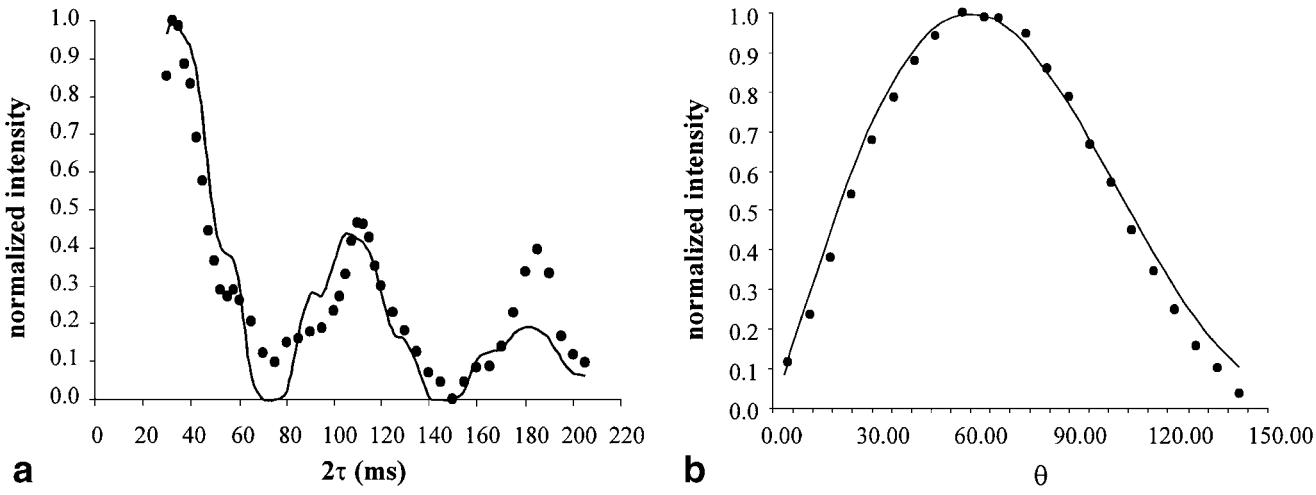

FIG 2. The dependence of the intensity of the taurine signal passing through the DQ filter on the DQ creation time 2τ (**a**) and on the flip angle (θ) of the DQ read pulse (**b**). Signal intensity was normalized to the maximum in each curve. In both **a** and **b**, solid circles represent experimental data acquired from phantom 1, whereas the solid lines were simulated by using Eq. [2] with T_2 = 178 msec (**a**) and Eq. [3] (**b**).

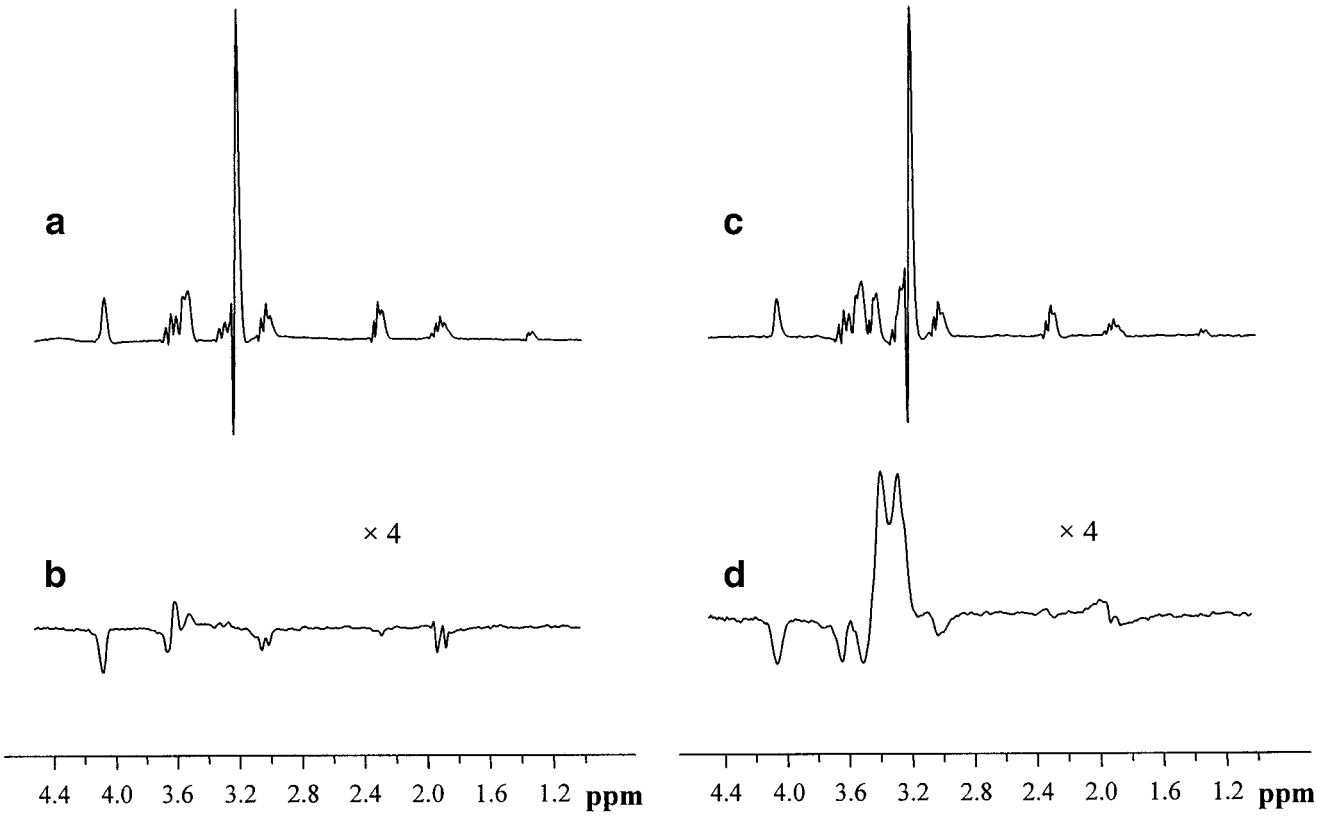

FIG 3. STEAM spectra without editing (**a** and **c**) and taurine-edited spectra (**b** and **d**) acquired from the same voxels located in the inner vial of the phantom 2 (**a** and **b**) and 3 (**c** and **d**).

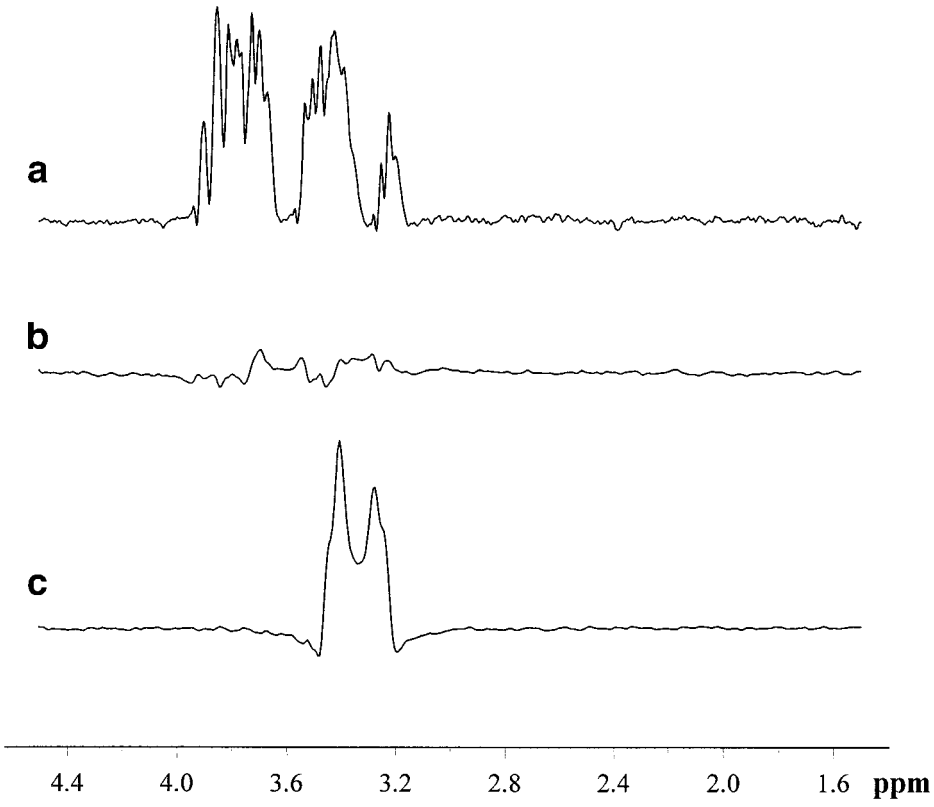

FIG 4. A STEAM spectrum acquired without taurine editing from a voxel located in the inner vial of phantom 4 (**a**) and a taurine-edited spectrum acquired from the same voxel (**b**), showing residual glucose signals passing through the taurine-editing DQ filter. A taurine-edited spectrum from a voxel of the same size located in the outer vial of the phantom is shown for comparison (**c**).

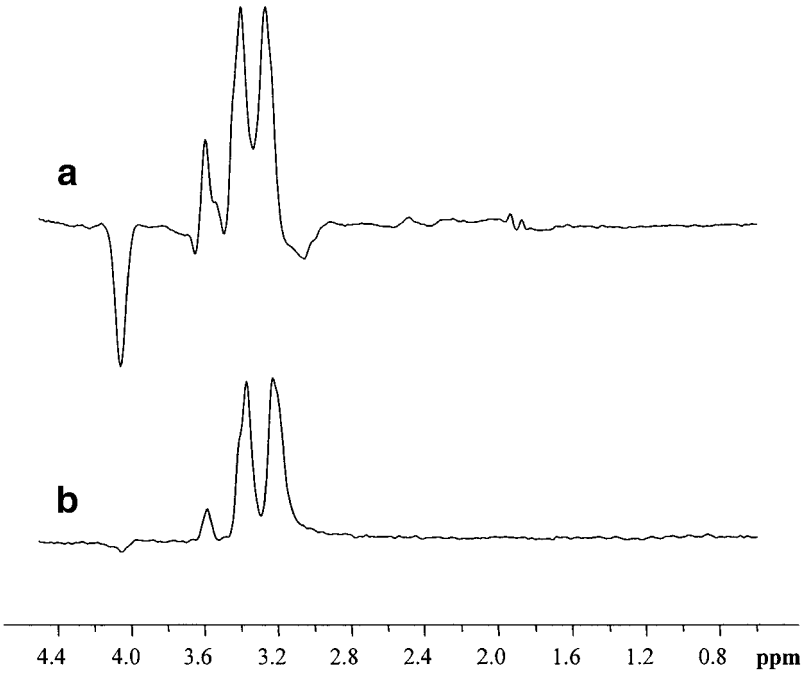

FIG 5. Taurine-edited spectra acquired from a voxel located in the inner vial of phantom 3. Spectrum **a** was acquired with the DQ-filtering sequence depicted in Fig. 1, whereas spectrum **b** was acquired with a DQ-filtering sequence that uses Gaussian pulses for excitation and DQ coherence creation and a hard DQ coherence read pulse (19). The intensity of the taurine peaks in **a** is 1.42-fold higher than that in **b**.

Nonedited and taurine-edited spectra acquired from the same voxel of a rat brain in vivo are shown in Fig. 6a and b, respectively, together with a taurine-edited spectrum acquired from another rat (Fig. 6c). The localized taurine-edited spectra are reproducible, and display features similar to those in spectra from phantoms.

DISCUSSION

Product operator formalisms have been used to design and optimize the performance of DQ-filtering sequences for weakly coupled spin systems such as lactate (30) and GABA (31) and for some simple strongly coupled spin systems such as citrate (15) and *N*-acetylaspartate (17). Lack of a spin-system-specific product operator formalism (26) for more complicated strongly coupled systems makes the design and optimization of DQ-filtering sequences difficult for such spin systems, although an alternate procedure for designing and optimizing DQ-filtering sequences for more complicated strongly coupled spin systems has been described and used to design a DQ-filtering sequence for selective observation of glutamate in vivo (18). The duration of the DQ coherence creation period (2τ) has significant effects on both the detection sensitivity (via

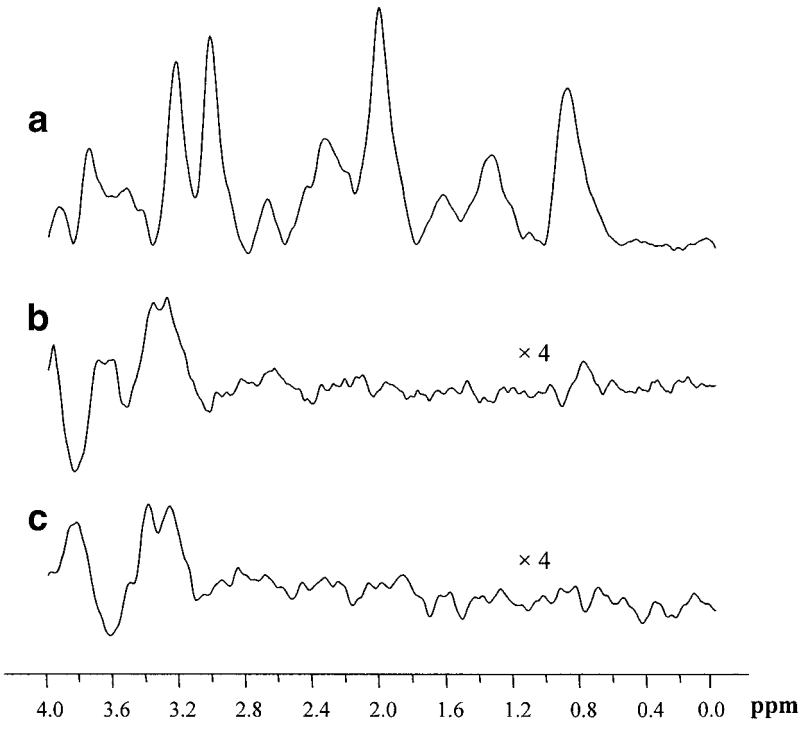

FIG 6. A STEAM spectrum obtained without spectral editing (**a**) from a rat brain in vivo and a taurine-edited spectrum (**b**) acquired from the same voxel. Spectrum **c** shows a taurine-edited spectrum acquired from an identical voxel in the brain of another rat. The intensity scale in **b** and **c** is 4 times that in **a**.

inherent yield and signal loss through transverse relaxation) and the line shape of the resulting signal (18). An exact product operator formalism for an A_2B_2 spin system has not been developed. Treating taurine as a weakly coupled (A_2X_2) spin system results in a large deviation between the theoretical response and the experimental response to the DQ-filtering sequence (19). In view of the assumptions made here, Eq. [2] should not be considered an exact 2τ dependence function for an A_2B_2 system. However, the 2τ dependence curve agrees very well with experiment, having calculated periodic local maxima and minima at $2\tau = (2k + 1)/4J$ and $2\tau = \pi k/\Lambda$, where $k = 0, 1, 2, 3 \ldots$, as observed experimentally. In particular, at 7 T the calculated 2τ value that gives the maximum taurine signal intensity occurs between 38.3 msec ($2\pi/\Lambda$) and 37.0 msec ($1/4J$), in accord with experiment.

The flip angle θ of the DQ coherence read pulse also affects the detection sensitivity (18,27). The 90 Hz bandwidth of the read pulse used in the experiments described here covers the frequency range of both taurine methylene groups at 7 T so that it converts the DQ coherence originating from both methylene groups into single quantum coherence. It can therefore be considered to be a non-frequency-selective read pulse, as required for Eq. [3]. Even though Eq. [3] was derived for an AX system (27), it also applies to AB systems (15), and excellent agreement with our experiment is shown here for the A_2B_2 system of taurine. In particular, the simulation and experiment agree that a 60° read pulse gives signal intensity 30% higher than a 90° pulse. When a hard pulse is used as the read pulse, the maximum taurine signal intensity occurs when the flip angle is 90° (19). The reason for this difference is not clear.

The sequence in Fig. 1 provides improved sensitivity over a DQ-filtering sequence that uses Gaussian pulses for excitation and DQ coherence creation and a hard DQ coherence read pulse. This can be important for in vivo applications. Long shaped pulses interact with J-coupled spin systems in a way that is quite different from short hard pulses (32). Nonnegligible unwanted coherences can be generated if soft pulses are used in a DQ-filtering sequence, reducing the efficiency of coherence transfer and resulting in significant signal loss (32), depending on the pulse time, coupling constants, and chemical shifts. Thus the use of more hard pulses as in the DQ-filtering sequence described here may produce more efficient coherence transfer and improved sensitivity. Furthermore, because a shorter shaped pulse is used, t_1 can be reduced, providing additional sensitivity through minimizing J-modulation effects during the t_1 period (11).

Although it is important to optimize the detection sensitivity of a DQ-filtering sequence, it is essential for the optimized DQ-filtering sequence to be efficient in filtering out major overlapping resonances from other metabolites, such as choline, *myo*-inositol, and glucose in the case of editing for taurine. The results of this study show that effective filtering is accomplished by using the DQ-filtering sequence depicted in Fig. 1. Several mechanisms contribute to the efficient filtering. First, because of the nature of DQ filtering, all singlets in the spectrum including those from choline at about 3.20 ppm will be suppressed completely. Second, the DQ coherence read pulse is made frequency-selective and excites only a narrow frequency window (90 Hz) around the taurine resonances so that the signals from coupled systems whose resonances do not all fall into that window will be completely suppressed (such as lactate and the choline methylene resonances at 3.54 ppm) or attenuated (*myo*-inositol, GABA, and glucose). Third, by using 2τ optimized for taurine, signals from metabolites falling into this window but having coupling constants different from that of taurine will be attenuated. Thus the signals of [H5] of *myo*-inositol at 3.28 ppm, which is coupled by 9.0 Hz to [H4,6] at 3.62 ppm (33), is suppressed almost completely. Substantial attenuation of glucose signals is also achieved through this mechanism since most of the coupling constants differ from those of taurine (16). Although most of the resonances that overlap with the taurine signals are suppressed through these three mechanisms, some still remain in the edited spectra, albeit with substantially reduced intensity. These include *myo*-inositol resonances at 3.59 ppm and 4.06 ppm, choline methylene resonances at 4.06 ppm, GABA resonances at 3.00 ppm, and glucose resonances between 3.20 and 3.80 ppm. Except for the glucose resonances, these all differ in chemical shift from the taurine resonances. Unless the shimming is very poor, they will not interfere with the observation of taurine and can be eliminated through postacquisition processing (14). However, when shimming is poor, as might be the case for in vivo editing, residual resonances of *myo*-inositol at 3.59 ppm could potentially overlap with the downfield taurine resonance. In the worst case, when the taurine resonances overlap completely with those of *myo*-inositol, the contribution of *myo*-inositol to the edited signals will be approximately 15% (Fig. 3b and d), assuming that taurine and *myo*-inositol are present at equal concentrations. Some of the glucose resonances that pass through the DQ filter have the same chemical shift as the taurine resonances and can obscure taurine observation. However, the relative detection sensitivity of the DQ-filtering sequence for glucose is only one-eighth of that for taurine. Furthermore, in tissues such as brain, the taurine concentration is higher than that of glucose under normal physiological conditions [e.g., 5.5 μmol/g (34–37) versus about 2.4 μmol/g (38) for rat brain]. Then the contribution of glucose to the in vivo MR spectrum of rat brain in Fig. 6 is probably only about 5%.

The first 90° pulse and the two 180° refocusing pulses in a DQ-filtering sequence can be made slice selective to achieve single-shot three dimensional (3D) localization in a manner that is similar to point resolved spectroscopy (PRESS) (12,14,18). However, the phase accumulation induced by slice-selective excitation and refocusing often creates problems (12). A phase correction procedure and the use of self-refocusing pulses have been proposed to solve this problem (14,18), but the robustness of these methods has not been demonstrated. The DQ-filtering sequence has also been combined with ISIS to achieve single voxel spatial localization (39). In the DQ-filtering sequence described here, slice-selective refocusing combined with the ISIS strategy is used to achieve effective 3D localization. Making the second 180° refocusing pulse of the DQ filter slice selective does not introduce a frequency offset-dependent (i.e., position-dependent) modulation of the edited signal intensity (12), so that no RF pulse phase adjustment is needed (14). By using two slice-selective

inversion pulses, in-plane localization is achieved in a manner that resembles ISIS (22). This localization strategy has advantages over conventional 3D ISIS. First, the use of two slice-selective inversion pulses instead of three reduces T_1 relaxation effects, thus improving sensitivity. Second, only four ISIS steps are required instead of eight to achieve 3D localization, thus reducing sensitivity to motion. Moreover, by switching the single band inversion pulses to multiple band inversion pulses and using Hadamard encoding, taurine editing with multiple-voxel in-plane localization can be obtained (40).

The DQ filter developed in this study is optimized for the selective observation of taurine at high field strength (7 T). Whether this sequence is applicable to human studies at lower field strength requires further investigation. The response of taurine to the DQ filter is field strength dependent, as are the responses of *myo*-inositol and glucose. Therefore, at lower field strength, the experimental parameters for optimized taurine editing could be different from those used in this study. Longer T_2 for the metabolites at lower field strength and the larger voxel size that can be used on human subjects will effectively increase the detection sensitivity.

ACKNOWLEDGMENTS

The authors thank Dr. D. Hardy for helpful discussions.

REFERENCES

1. Lombardini JB, Schaffer SW, Azuma J, eds. Taurine: nutritional value and mechanisms of action. Adv Exp Med Biol 1991;315.
2. Huxtable RJ, Michalk D, eds. Taurine in health and disease. Adv Exp Med Biol 1993;359.
3. Huxtable RJ, Azuma J, Kuriyama K, Nakagawa M, Baba A, eds. Taurine 2: Basic and clinical aspects. Adv Exp Med Biol 1995;403.
4. Michaelis T, Merboldt KD, Hanicke W, Gyngell ML, Bruhn H, Frahm J. On the identification of cerebral metabolites in localized ^{1}H NMR spectra of human brain in vivo. NMR Biomed 1991;4:90–98.
5. Bates TE, Williams SR, Gadian DG, Bell JD, Small RK, Iles RA. ^{1}H NMR study of cerebral development in the rat. NMR Biomed 1989;2:225–229.
6. Hida K, Kwee IL, Nakada T. In vivo ^{1}H and ^{31}P NMR spectroscopy of the developing rat brain. Magn Reson Med 1992;23:31–36.
7. Brulatout S, Meric P, Loubinoux I, Borredon J, Correze JL, Roucher P, Gillet B, Berenger G, Beloeil JC, Tiffon B, Mispelter J, Seylaz J. A one-dimensional (proton and phosphorus) and two-dimensional (proton) in vivo NMR spectroscopic study of reversible global cerebral ischemia. J Neurochem 1996;66:2491–2499.
8. Barrere B, Peres M, Gillet B, Mergui S, Beloeil JC, Seylaz J. 2D COSY ^{1}H NMR: a new tool for studying *in situ* brain metabolism in the living animal. FEBS Lett 1990;264:198–202.
9. Remy C, Arus C, Ziegler A, Lai ES, Moreno A, Le Fur Y, Decorps M. In vivo, *ex vivo*, and *in vitro* one- and two-dimensional nuclear magnetic resonance spectroscopy of an intracerebral glioma in rat brain: assignment of resonances. J Neurochem 1994;62:166–179.
10. Rothman DL, Behar KL, Hetherington HP, Shulman RG. Homonuclear ^{1}H double-resonance difference spectroscopy of the rat brain in vivo. Proc Natl Acad Sci USA 1984;81:6330–6334.
11. van Dijk JE, Mehlkopf AF, Bovee WM. Comparison of double and zero quantum NMR editing techniques for in vivo use. NMR Biomed 1992;5:75–86.
12. Jouvensal L, Carlier PG, Bloch G. Practical implementation of single-voxel double-quantum editing on a whole-body NMR spectrometer: localized monitoring of lactate in the human leg during and after exercise. Magn Reson Med 1996;36:487–490.
13. He Q, Shungu DC, van Zijl PC, Bhujwalla ZM, Glickson JD. Single-scan in vivo lactate editing with complete lipid and water suppression by selective multiple quantum coherence transfer (Sel-MQC) with application to tumors. J Magn Reson B 1995;106:203–211.
14. Keltner JR, Wald LL, Frederick BD, Renshaw PF. In vivo detection of GABA in human brain using a localized double-quantum filter technique. Magn Reson Med 1997;37:366–371.
15. Wilman AH, Allen PS. Double-quantum filtering of citrate for in vivo observation. J Magn Reson B 1994;105:58–60.
16. Keltner JR, Wald LL, Ledden PJ, Chen YC, Matthews RT, Kuestermann EH, Baker JR, Rosen BR, Jenkins BG. A localized double-quantum filter for the in vivo detection of brain glucose. Magn Reson Med 1998;39:651–656.
17. Wilman AH, Allen PS. Observing *N*-acetyl aspartate via both its *N*-acetyl and its strongly coupled aspartate groups in in vivo proton magnetic resonance spectroscopy. J Magn Reson B 1996;113:203–213.
18. Thompson RB, Allen PS. A new multiple quantum filter design procedure for use on strongly coupled spin systems found in vivo: its application to glutamate. Magn Reson Med 1998;39:762–771.
19. Hardy DL, Norwood TJ. Spectral editing technique for the *in vitro* and in vivo detection of taurine. J Magn Reson 1998;133:70–78.
20. Perman WH, Bernstein MA, Sandstrom JC. A method for correctly setting the rf flip angle. Magn Reson Med 1989;9:16–24.
21. Silver MS, Joseph RI, Hoult DI. Highly selective $\pi/2$ and π pulse generation. J Magn Reson 1984;59:347–351.
22. Ordidge RJ, Bowley RM, McHale G. A general approach to selection of multiple cubic volume elements using the ISIS technique. Magn Reson Med 1988;8:323–331.
23. van Zijl PC, Johnson MO, Mori S, Hurd RE. Magic-angle-gradient double-quantum-filtered COSY. J Magn Reson A 1995;113:265–270.
24. Haase A. Snapshot FLASH MRI. Applications to T1, T2, and chemical-shift imaging. Magn Reson Med 1990;13:77–89.
25. Frahm J, Merboldt KD, Hanicke W. Localized proton spectroscopy using stimulated echoes. J Magn Reson 1987;72:502–508.
26. Kay LE, McClung RED. A product operator description of AB and ABX spin systems. J Magn Reson 1988;77:258–273.
27. Shen JF, Allen PS. Enhancement of double-quantum-filtered signals using optimized tip angle RF pulses. J Magn Reson 1990;90:606–611.
28. Shen JF, Allen PS. Reduced length for double-quantum filtering sequences. J Magn Reson 1991;92:398–403.
29. Behar KL, Ogino T. Assignment of resonance in the ^{1}H spectrum of rat brain by two-dimensional shift correlated and J-resolved NMR spectroscopy. Magn Reson Med 1991;17:285–303.
30. Nosel W, Trimble LA, Shen JF, Allen PS. On the use of double-quantum coherence from an AX_3 system (protons in lactate) for spectral editing. Magn Reson Med 1989;11:398–404.
31. Wilman AH, Allen PS. In vivo NMR detection strategies for gamma-aminobutyric acid, utilizing proton spectroscopy and coherence-pathway filtering with gradients. J Magn Reson B 1993;101:165–171.
32. Slotboom J, Mehlkopf AF, Bovee WM. The effects of frequency-selective RF pulses on J-coupled spin-systems. J Magn Reson A 1994;108:38–50.
33. Cerdan S, Parrilla R, Santoro J, Rico M. ^{1}H NMR detection of cerebral *myo*-inositol. FEBS Lett 1985;187:167–172.
34. Puka M, Sundell K, Lazarewicz JW, Lehmann A. Species differences in cerebral taurine concentrations correlate with brain water content. Brain Res 1991;548:267–272.
35. Chapman AG, Westerberg E, Premachandra M, Meldrum BS. Changes in regional neurotransmitter amino acid levels in rat brain during seizures induced by L-allylglycine, bicuculline, and kainic acid. J Neurochem 1984;43:62–70.
36. Korpi ER, Wyatt RJ. Effects of chronic D-amphetamine and phenylethylamine on the concentrations of neurotransmitter amino acids in the rat brain. Int J Neurosci 1983;18:239–246.
37. Durkin TA, Anderson GM, Cohen DJ. High-performance liquid chromatographic analysis of neurotransmitter amino acids in brain. J Chromatogr 1988;428:9–15.
38. Wagner SR, Lanier WL. Metabolism of glucose, glycogen, and high-energy phosphates during complete cerebral ischemia. A comparison of normoglycemic, chronically hyperglycemic diabetic, and acutely hyperglycemic nondiabetic rats. Anesthesiology 1994;81:1516–1526.
39. Thomas MA, Hetherington HP, Meyerhoff DJ, Twieg DB. Localized double quantum filtered ^{1}H NMR spectroscopy. J Magn Reson 1991;93:485–496.
40. Gonen O, Hu J, Stoyanova R, Leigh JS, Goelman G, Brown TR, Walter G. Hybrid three dimensional (1D-Hadamard, 2D-chemical shift imaging) phosphorus localized spectroscopy of phantom and human brain Hadamard spectroscopic imaging technique as applied to study human calf muscles. Magn Reson Med 1992;25:349–354.